mathematics

MDPI

Article

Charged Cavitation Multibubbles Dynamics Model: Growth Process

Ahmed K. Abu-Nab [1,2,*], Amerah M. Hakami [3] and Ali F. Abu-Bakr [1]

[1] Department of Mathematics and Computer Science, Faculty of Science, Menoufia University, Shebin El-Koom 32511, Egypt; alibakrm@yahoo.com
[2] Moscow Institute of Physics and Technology, Phystech School of Applied Mathematics and Informatics, Dolgoprudny 141700, Russia
[3] Department of Mathematics, Faculty of Science, Jazan University, Jazan 82723, Saudi Arabia; amhakami806@gmail.com
* Correspondence: ahmed.abunab@yahoo.com or ahmed.kamal87@science.menofia.edu.eg; Tel.: +20-1092568892

Abstract: The nonlinear dynamics of charged cavitation bubbles are investigated theoretically and analytically in this study through the Rayleigh–Plesset model in dielectric liquids. The physical and mathematical situations consist of two models: the first one is noninteracting charged cavitation bubbles (like single cavitation bubble) and the second one is interacting charged cavitation bubbles. The proposed models are formulated and solved analytically based on the Plesset–Zwick technique. The study examines the behaviour of charged cavitation bubble growth processes under the influence of the polytropic exponent, the number of bubbles N, and the distance between the bubbles. From our analysis, it is observed that the radius of charged cavitation bubbles increases with increases in the distance between the bubbles, dimensionless phase transition criteria, and thermal diffusivity, and is inversely proportional to the polytropic exponent and the number of bubbles N. Additionally, it is evident that the growth process of charged cavitation bubbles is enhanced significantly when the number of bubbles is reduced. The electric charges and polytropic exponent weakens the growth process of charged bubbles in dielectric liquids. The obtained results are compared with experimental and theoretical previous works to validate the given solutions of the presented models of noninteraction and interparticle interaction of charged cavitation bubbles.

Keywords: charged bubbles; interparticle interaction; growth process; analytical solution; Plesset–Zwick technique

MSC: 76M35; 35Q31; 35Q05; 76M20

Citation: Abu-Nab, A.K.; Hakami, A.M.; Abu-Bakr, A.F. Charged Cavitation Multibubbles Dynamics Model: Growth Process. *Mathematics* **2024**, *12*, 569. https://doi.org/10.3390/math12040569

Academic Editor: Arsen Palestini

Received: 4 January 2024
Revised: 19 January 2024
Accepted: 25 January 2024
Published: 14 February 2024

1. Introduction

Cavitation bubbles dynamics is a basic scientific subject with many fascinating and intricate dynamical properties that are of general interest [1]. More than a hundred years ago, many scientists and researchers began studying cavitation bubble dynamics and their potential uses in an attempt to reduce damage to ship propellers. Since then, bubbles have attracted enormous scientific and technological interest [2,3]. Many significant applications arise from cavitation bubble dynamics, which exhibit volumetric oscillations because of pressure imbalances. Different dynamic pressure imbalances give rise to bubbles of different cavitations, which exhibit numerous volumetric oscillations that have a wide range of use in many important applications. Certain acoustic and induced-laser cavitation bubbles [4–6], for instance, are used for medication and gene delivery [7,8], therapeutic biological systems [9–12], ultrasonic cleaning [13], sonoluminescence [14], inkjet printing [15], and bubble propulsion [16]. The efforts of researchers [1–15] help the researchers to understand and develop the bubble dynamics and its application, so these results enhance the scientific fields.

The cavitation bubbles are usually millimetre- or micrometre-sized oscillating bubbles. Air weapon bubbles and submerged blast bubbles, which can be metre-size-varying bubbles, are essential elements used in underwater implosion and geophysical studies [16,17]. Moreover, oscillating bubbles that range in size from millimetres to metres, known as hydraulic bubbles, trapped air bubbles, and heat-generated steam bubbles, can play a significant role in the operation of engines, reactors, and turbines [18,19]. Many research projects and applications are still being conducted on the use of bubble dynamics in discoveries and different applications for bubbles of different sizes.

Science started looking at bubble dynamics theoretically in the early 20th century. The Rayleigh–Plesset equation was derived, which is a classical equation that provides an accurate description of the oscillation of bubbles in incompressible fluids [20]. The Rayleigh–Plesset equation did not take into account energy lost due to acoustic frequencies, such as pressure waves resulting from the collapse of a bubble, as it relied on incompressible fluids. As a result, this equation becomes inappropriate when the collapse in the bubble radius or the energy lost is important and cannot be neglected. Weakly compressible bubble models were established, taking into account the weak compressibility of the fluid outside the bubble. The most widely used of them was the Keller–Mikis model [21], which was developed using the incompressible Bernoulli equation and the wave equation. Based on perturbation theory, Prosperetti and Lezzi [22,23] proposed a new model for describing behaviour dynamics that took the fluid's compressibility into account. Subsequently, many different models [24–26] were presented that made a significant contribution to theoretical studies of bubble dynamics in compressible fluids.

It is notable that, because bubbles have multiple oscillation cycles, boundaries, and scales, their dynamics are complex and present significant challenges for theoretical, numerical, and experimental research, regardless of whether the bubbles originate from natural or artificial sources. Understanding the physics of bubbles under various conditions and the basis for deciphering and comprehending a wide range of bubble dynamics and behaviour phenomena, as well as how they can be used in diverse industrial and biological applications, depend heavily on theoretical research. Recently, bubble dynamics [27] were investigated theoretically under consideration of the effect of magnetic field and liquid electrical conductivity where the authors [27] obtained the analytical results of the behaviour of single bubble dynamics in a generalized Newtonian fluid, especially how the impact of magnetic field weakens the gas bubble growth. Additionally, the development and application of analytical and numerical methods to study bubble dynamics in mathematical models has garnered increased attention in the last few years [28–33].

To the best of our knowledge, the mathematical models of bubbles used in all prior research on how frequencies affect the behaviour of multibubbles were considered, demonstrating that these bubbles are not charged. However, it has been shown that when exposed to acoustic forces, air and gas bubbles in liquids are electrostatically charged. A long-standing issue is the charging deposition on bubbles at bubble–liquid interfaces [34,35]. Experimental evidence has confirmed that the phenomena is related to the movement of ionic charge from the liquid onto the surface of the bubble. The dynamics of driven charged bubbles remain poorly understood, although charged bubbles have numerous potential uses in the creation of electro-aerosol sprays, which are made of highly charged particles, wastewater treatment [36], biological medicine [37], and the production of food [38].

Additionally, significant progress was made when the modified Rayleigh–Plesset equation for an acoustically single-frequency generated gas bubble was used, taking into account the existence of charge Q on the bubble's surface. When a charged bubble is present, its effective surface tension is lowered, which causes the bubble to enlarge in radius and then rapidly collapse to a minimal radius. Furthermore, it was observed that the charge raises the maximum achievable bubble radius and accelerates the occurrence of the period-doubling-bifurcations route to chaos [39].

The goal of this work is to present the theoretical and analytical study of nonlinear dynamics of charged bubbles. The study investigates the noninteracting and interacting

charged cavitation bubbles in dielectric liquids where the proposed models are solved analytically based on the Plesset–Zwick method. The validation and verification of the proposed models are discussed in the text. A graphic representation of the results is estimated by Mathematica software (ver.13.1). The comparison between the current model with available published results are revealed in this study.

2. Model

This investigation highlights the significance of nonlinear Rayleigh–Plesset differential equations in comprehending complexity and intricate phenomena and treatment processes across different applied sciences. It is found that several mathematical and physical approaches are discussed to investigate nonlinear Rayleigh–Plesset differential equations, including numerical solutions, linearization methods, quadrature solutions, asymptotic analysis, and analytical solutions, which are investigated in our study. The analytical study of nonlinear dynamics of charged cavitation bubbles is introduced in dielectric liquids. For that, the physical problem is analysed in Figure 1, where the charged cavitation bubbles are in the dielectric liquid. This is supposing that the translational motion of charged bubbles and gravity force are neglected. The current physical situation has two models: the first model is to study the noninteracting, charged cavitation bubbles and the second one is in the case of interacting, charged cavitation bubbles. The proposed model is formulated, solved, and discussed in further sections.

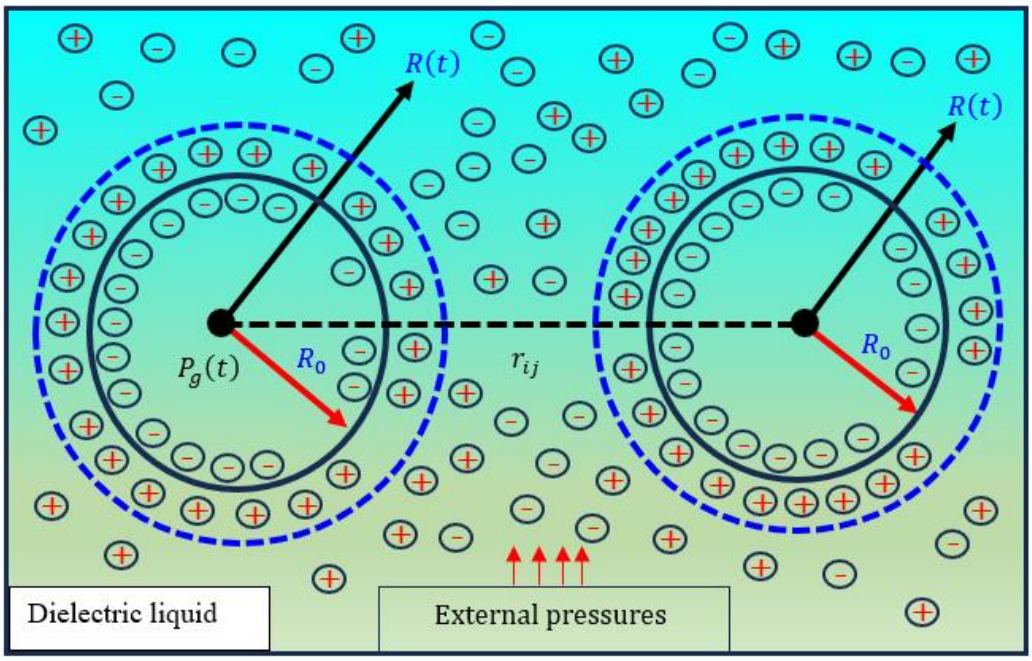

Figure 1. Sketch charged multibubbles dynamics; $(+)$ and $(-)$ are the positive and negative of electric charges. External pressures are defined in the text.

2.1. Noninteraction-Charged Cavitation Bubble

In our approach, the mechanism of charged cavitation microbubble dynamics occurs in a viscous mixture of vapour and superheated, incompressible Newtonian fluid between a two-phase flow (namely, an extended charged-Rayleigh–Plesset model) [39,40] can be expressed as:

$$\rho(R\ddot{R} + \frac{3}{2}\dot{R^2}) = \left(P_k + P_\eta + P_\sigma + P_Q + (P_v - P_0)\right). \quad (1)$$

Here, P_k is the pressure due to polytropic effects, which can be expressed in charged liquid as:

$$P_k = \left(P_v - P_0 + \frac{2\sigma}{R_0} - \frac{Q^2}{8\pi\varepsilon R_0^4}\right)\left(\frac{R_0}{R}\right)^{3\kappa} \text{ and } \kappa = \begin{cases} 1 \\ \frac{4}{3} \text{ or } \frac{5}{3} \end{cases} \tag{2}$$

Moreover, P_σ and P_η refer to the acting pressures because of the forces of the surface tension and viscous effects, respectively, which can be read as:

$$P_\sigma = \frac{2}{R}\sigma. \tag{3}$$

and

$$P_\eta = 4\frac{\dot{R}}{R}\eta, \tag{4}$$

where σ is the surface tension. η is the viscosity dynamic.

In our study, P_Q is the charged pressure in the permittivity of the dielectric space-filling liquid ε in the system of dielectric liquid, which is defined as:

$$P_Q = \frac{Q^2}{8\pi\varepsilon R^4} \tag{5}$$

Here, Q is the electric charge. $\varepsilon = 85\ \varepsilon_0$; ε_0 refers to initial permittivity.

Combining Equations (1)–(5), the charged-Rayleigh–Plesset model in dielectric liquid for charged single cavitation bubble becomes:

$$\rho(R\ddot{R} + \frac{3}{2}\dot{R^2}) = \left(\left(P_v - P_0 + \frac{2\sigma}{R_0} - \frac{Q^2}{8\pi\varepsilon R_0^4}\right)\left(\frac{R_0}{R}\right)^{3\kappa} - \frac{2}{R}\sigma - 4\frac{\rho\dot{R}}{R}\eta + \frac{Q^2}{8\pi\varepsilon R^4} + (P_v - P_0)\right). \tag{6}$$

The pressure of the charged bubbles [8] $P_g(t)$ can be expressed as:

$$P_g(t) = \left(P_v - P_0 + \frac{2\sigma}{R_0}\right)\left(\frac{R_0}{R}\right)^{3\kappa}. \tag{7}$$

From Equations (6)–(8), Equation (6) becomes:

$$R\ddot{R} + \frac{3}{2}\dot{R^2} = \frac{1}{\rho}(P_g(t) - P_0) - \frac{Q^2}{8\pi\rho\varepsilon R_0^4}\left(\frac{R_0}{R}\right)^{3\kappa} - 4\frac{\dot{R}}{R}\eta - \frac{2}{\rho R}\sigma + \frac{Q^2}{8\pi\rho\varepsilon R^4} + \frac{1}{\rho}P_v. \tag{8}$$

The pressure difference [41] $(P_g(t) - P_0)$ can be stated as:

$$P_g(t) - P_0 = \mathbb{Z}_1(T_R(t) - T_s), \tag{9}$$

where $\mathbb{Z}_1$ defines a constant, which will be calculated below. T_b and T_s are the instantaneous temperature of the gas surrounding the charged bubble and the saturation temperature, respectively.

Combing Equations (8) and (9), Equation (8) becomes:

$$R\ddot{R} + \frac{3}{2}\dot{R^2} = \frac{1}{\rho}\mathbb{Z}_1(T_b(t) - T_s) - \frac{Q^2}{8\pi\rho\varepsilon R_0^4}\left(\frac{R_0}{R}\right)^{3\kappa} - 4\frac{\dot{R}}{R}\eta - \frac{2}{\rho R}\sigma + \frac{Q^2}{8\pi\rho\varepsilon R^4} + \frac{1}{\rho}P_v. \tag{10}$$

The approach can be solved by taking the initial and boundary conditions into account, which can be expressed as:

$$R(t_0) = R_0, \dot{R}(t_0) = \dot{R}_0, \ddot{R}(t_0) = 0,\ T_R(t_0) = T_0, \tag{11}$$

$$R(t_m) = R_m, \dot{R}(t_m) = \dot{R}_m, \ddot{R}(t_m) = 0, \tag{12}$$

where 0 and m represent, respectively, the initial and maximum values. Applying the condition (9) into (10), the $\mathbb{Z}_1$ becomes:

$$\mathbb{Z}_1 = \frac{\mathbb{Z}_2}{T_0 - T_\infty}; \tag{13}$$

$$\mathbb{Z}_2 = \frac{3}{2}\rho\dot{R}_0^2 + 4\frac{\rho\dot{R}_0}{R_0}\eta + \frac{2}{R_0}\sigma - P_v.$$

Combining Equations (10) and (12), Equation (10) takes this form:

$$R\ddot{R} + \frac{3}{2}\dot{R}^2 = \frac{1}{\rho}\left(\frac{\Delta T_B^*}{\Delta T_0} + 1\right)\mathbb{Z}_2 - \frac{Q^2}{8\pi\rho\varepsilon R_0^4}\left(\frac{R_0}{R}\right)^{3\kappa} - 4\frac{\dot{R}}{R}\eta - \frac{2}{\rho R}\sigma + \frac{Q^2}{8\pi\rho\varepsilon R^4} + \frac{1}{\rho}P_v. \tag{14}$$

Here $R\ddot{R} + \frac{3}{2}\dot{R}^2 = \frac{1}{2R^2\dot{R}}\frac{d}{dt}\left(R^3\dot{R}^2\right)$, $\Delta T_0 = T_0 - T_\infty$; is the initial value of over-temperature and ΔT_T^* is the solution of temperature equation (i.e., [42–44]), which stated as:

$$\Delta T_B^* = T_R - T_0 = -\left(\frac{a_l}{\pi}\right)^{\frac{1}{2}}\int_0^t\left(\left(\int_0^t R^4(x_2)dx_2\right)^{-1/2}\left(R^2(x_1)\left(\frac{\partial T}{\partial r}\right)_{r=R(x)}\right)\right)dx_1, \tag{15}$$

where a_l is the diffusion coefficient.

The temperature gradient $\frac{\partial T}{\partial r}$ can be evaluated via the equilibrium of gas diffusion at the microbubble wall [43] as follows:

$$\left(\frac{\partial T}{\partial r}\right)_{r=RS} = \frac{4}{3}\pi\frac{\frac{d}{dt}(\rho_g R^3)}{a_l A};\ A = 4\pi R^2. \tag{16}$$

Here A is the surface area of bubble. $\frac{\partial T}{\partial r}$ is the concentration gradient at the surface of bubble. T defines the temperature of the given medium. To complete the solution, Equation (16) is transformed to a dimensionless equation, via which aids these transformations as:

$$\Psi = \left(\frac{R}{R_0}\right)^3, \nu = \frac{\Omega}{R_0^4}\int_0^t R^4(x_2)dx_2, \Omega = \sqrt{\frac{2R}{\rho_L R_0^3}}., \frac{ds}{dt} = \frac{1}{3}\Omega R_0\Psi^{\frac{2}{3}}\Psi', \frac{d^2R}{dt^2} = \frac{1}{3}\Omega^2 R_0\Psi\left(\Psi\Psi'' + \frac{2}{3}\Psi'^2\right). \tag{17}$$

On the other hand, we can convert ΔT_B^* and $\left(\frac{\partial T}{\partial r}\right)_{r=S}$ in dimensionless forms.

$$\left.\begin{array}{c}\Delta T_B^* = -\frac{\rho_v R_0}{3a_l}\left(\frac{\Omega a_l}{\pi}\right)^{\frac{1}{2}}\int_0^\nu\left((\nu-\xi)^{-\frac{1}{2}}\Psi(\xi)\right)d\xi \\ \left(\frac{\partial T}{\partial r}\right)_{r=S} = \frac{S_0\rho_g}{3a_l}\Omega\Psi^{\frac{2}{3}}\Psi\end{array}\right\}. \tag{18}$$

With help via Equations (17) and (18), Equation (13) can be put in a dimensionless equation as:

$$\frac{1}{6\Psi'}\frac{d}{d\nu}\left(\Psi^{\frac{7}{3}}\Psi'^2\right) = \frac{1}{\rho\Omega^2R_0^2}\mathbb{Z}_2 - \mathbb{Z}_3\int_0^\nu\left((\nu-\xi)^{-\frac{1}{2}}\Psi'(\xi)\right)d\xi - \frac{Q^2}{8\pi\rho\varepsilon\Omega^2R_0^2}\left(\frac{1}{\Psi^{\frac{1}{3}}}\right)^{3\kappa} - \frac{4}{3}\frac{4}{\Omega R_0^2}\Psi^{\frac{1}{3}}\Psi'\eta - \frac{2}{\rho\Omega^2R_0^2}\frac{1}{\Psi^{\frac{1}{3}}}\sigma + \frac{Q^2}{8\pi\rho\varepsilon\Omega^2R_0^2}\frac{1}{\Psi^{\frac{1}{3}}} + \frac{1}{\rho\Omega^2R_0^2}P_v \tag{19}$$

where $\mathbb{Z}_3 = \left(\frac{\Omega a_l}{9\pi}\right)^{\frac{1}{2}}\frac{\rho_v L\mathbb{Z}_2}{\rho\Omega^2\Delta T_0 R_0 k_l}$.

When the charged microbubble dynamics are a complete growth, the inertial forces are neglected and the boundary conditions in Equation (11) are verified. Mathematically, these mean $R(t_m) = R_m, \dot{R}(t_m) = \dot{R}_m, \ddot{R}(t_m) = 0$ and $\frac{1}{6\Psi'}\frac{d}{d\nu}\left(\Psi^{\frac{7}{3}}\Psi'^2\right) \to 0$. Then, Equation (19) reduces to:

$$\int_0^{\nu}\left((\nu-\xi)^{-\frac{1}{2}}\Psi'(\xi)\right)d\xi=\frac{1}{\mathbb{Z}_3}\left[\frac{1}{\rho\Omega^2R_0^2}\mathbb{Z}_2-\frac{Q^2}{8\pi\rho\varepsilon\Omega^2R_0^2}\left(\frac{1}{\Psi_m^{\frac{1}{3}}}\right)^{3\kappa}-\frac{4}{3\Omega R_0^2}\Psi_m^{\frac{1}{3}}\Psi'_m\eta-\frac{2}{\rho\Omega^2R_0^2}\frac{1}{\Psi_m^{\frac{1}{3}}}\sigma+\frac{Q^2}{8\pi\rho\varepsilon\Omega^2R_0^2}\frac{1}{\Psi_m^{\frac{1}{3}}}+\frac{1}{\rho\Omega^2R_0^2}P_v\right] \tag{20}$$

To complete the solution of Equation (20), we use these assumptions: $\xi=\xi_1\nu$, and $\beta(\nu)=\gamma\nu^{\frac{1}{2}}$; γ denotes a constant, we obtain:

$$\gamma=\frac{2}{\mathbb{Z}_3\pi}\left[\frac{1}{\rho\Omega^2R_0^2}\mathbb{Z}_2-\frac{Q^2}{8\pi\rho\varepsilon\Omega^2R_0^2}\left(\frac{1}{\Psi_m^{\frac{1}{3}}}\right)^{3\kappa}-\frac{4}{3\Omega R_0^2}\Psi_m^{\frac{1}{3}}\Psi'_m\eta-\frac{2}{\rho\Omega^2R_0^2}\frac{1}{\Psi_m^{\frac{1}{3}}}\sigma+\frac{Q^2}{8\pi\rho\varepsilon\Omega^2R_0^2}\frac{1}{\Psi_m^{\frac{1}{3}}}+\frac{1}{\rho\Omega^2R_0^2}P_v\right]. \tag{21}$$

Then $\beta(\nu)$ becomes:

$$\beta(\nu)=\frac{2}{\mathbb{Z}_3\pi}\left[\frac{1}{\rho\Omega^2R_0^2}\mathbb{Z}_2-\frac{Q^2}{8\pi\rho\varepsilon\Omega^2R_0^2}\left(\frac{1}{\Psi_m^{\frac{1}{3}}}\right)^{3\kappa}-\frac{4}{3\Omega R_0^2}\Psi_m^{\frac{1}{3}}\Psi'_m\eta-\frac{2}{\rho\Omega^2R_0^2}\frac{1}{\Psi_m^{\frac{1}{3}}}\sigma+\frac{Q^2}{8\pi\rho\varepsilon\Omega^2R_0^2}\frac{1}{\Psi_m^{\frac{1}{3}}}+\frac{1}{\rho\Omega^2R_0^2}P_v\right]\nu^{\frac{1}{2}} \tag{22}$$

Applying Equation (22) into $R=R_0\Psi^{\frac{1}{3}}$, the charged microbubble radius becomes:

$$R=R_0\left[\frac{2}{\mathbb{Z}_3\pi}\left[\frac{1}{\rho\Omega^2R_0^2}\mathbb{Z}_2-\frac{Q^2}{8\pi\rho\varepsilon\Omega^2R_0^2}\left(\frac{1}{\Psi_m^{\frac{1}{3}}}\right)^{3\kappa}-\frac{4}{3\Omega R_0^2}\Psi_m^{\frac{1}{3}}\Psi'_m\eta-\frac{2}{\rho\Omega^2R_0^2}\frac{1}{\Psi_m^{\frac{1}{3}}}\sigma+\frac{Q^2}{8\pi\rho\varepsilon\Omega^2R_0^2}\frac{1}{\Psi_m^{\frac{1}{3}}}+\frac{1}{\rho\Omega^2R_0^2}P_v\right]\right]^{1/3}\nu^{\frac{1}{6}} \tag{23}$$

To introduce ν versus time t, Equation (23) is utilized into Equation (17), the result is defined as:

$$\nu^{\frac{1}{6}}=\left(\frac{\Omega}{3}t\right)^{\frac{1}{2}}\left[\frac{2}{\pi\mathcal{L}_2}\left[\frac{1}{\rho\Omega^2R_0^2}\mathbb{Z}_2-\frac{Q^2}{8\pi\rho\varepsilon\Omega^2R_0^2}\left(\frac{1}{\Psi_m^{\frac{1}{3}}}\right)^{3\kappa}-\frac{4}{3\Omega R_0^2}\Psi_m^{\frac{1}{3}}\Psi'_m\eta-\frac{2}{\rho\Omega^2R_0^2}\frac{1}{\Psi_m^{\frac{1}{3}}}\sigma+\frac{Q^2}{8\pi\rho\varepsilon\Omega^2R_0^2}\frac{1}{\Psi_m^{\frac{1}{3}}}+\frac{1}{\rho\Omega^2R_0^2}P_v\right]\right]^{2/3} \tag{24}$$

The charged noninteracting microbubble radius can be calculated as:

$$R=\left[\frac{2}{\mathbb{Z}_3\pi}\left[\frac{1}{\rho\Omega^2R_0^2}\mathbb{Z}_2-\frac{Q^2}{8\pi\rho\varepsilon\Omega^2R_0^2}\left(\frac{1}{\Psi_m^{\frac{1}{3}}}\right)^{3\kappa}-\frac{4}{3\Omega R_0^2}\Psi_m^{\frac{1}{3}}\Psi'_m\eta-\frac{2}{\rho\Omega^2R_0^2}\frac{1}{\Psi_m^{\frac{1}{3}}}\sigma+\frac{Q^2}{8\pi\rho\varepsilon\Omega^2R_0^2}\frac{1}{\Psi_m^{\frac{1}{3}}}+\frac{1}{\rho\Omega^2R_0^2}P_v\right]\right]^{1/3}\left(\frac{2}{\mathbb{Z}_3\pi}\right)^{\frac{2}{3}}\left(\frac{\Omega}{3}\right)^{\frac{1}{2}}t^{\frac{1}{2}} \tag{25}$$

From Equation (25), the charged noninteracting microbubble radius becomes:

$$R=\left[\frac{2}{\mathbb{Z}_3\pi}\left[\frac{1}{\rho\Omega^2R_0^2}\mathbb{Z}_2-\frac{Q^2}{8\pi\rho\varepsilon\Omega^2R_0^2}(\phi_0)^{\kappa}-\frac{4}{3\Omega R_0^2}\phi_0^{\frac{-1}{3}}\Psi'_m\eta-\frac{2}{\rho\Omega^2R_0^2}\phi_0^{\frac{1}{3}}\sigma+\frac{Q^2}{8\pi\rho\varepsilon\Omega^2R_0^2}\phi_0^{\frac{1}{3}}+\frac{1}{\rho\Omega^2R_0^2}P_v\right]\right]^{1/3}\frac{\Omega^2\rho R_0}{\mathbb{Z}_3}\left(\frac{12a_l}{3}\right)^{\frac{1}{2}}J_at^{\frac{1}{2}} \tag{26}$$

Here, the Jacob number ($J_a=\frac{\rho C_p\Delta T_0}{\rho_v L}$), thermal diffusivity ($a_l=\frac{k_l}{\rho C_p}$), and the initial void fraction can be defined as the ratio between the initial of the charged bubbles and the maximum volume of charged bubbles, which takes this form: $\phi_0=\left(\frac{R_0}{R_m}\right)^3$. It is noted that the charged cavitation bubbles are generated, and appear when this constraint ($0<\phi_0<1$) is satisfied.

2.2. Charged Cavitation Multibubble

In this section, the pressure due to the interparticle interaction of the cavitation of multibubbles and the model of the charged cavitation of multibubble is derived, then the pressure utilized in the spherical charged bubbles, respective to the volume modification, can be used to find the incompressible dielectric fluid and continuity with the equations of Euler [45] as follows:

$$\frac{\partial v}{\partial t}+v\frac{\partial v}{\partial r}=-\frac{1}{\rho}\nabla P, \tag{27a}$$

$$\frac{\partial v}{\partial r}+\frac{2}{r}v=0, \tag{27b}$$

where $v(r,t)$ is the fluid velocity, $P(r,t)$ is the pressure in the dielectric fluids, and r is the distance from the center of the charged bubble. ∇P is the gradient function of the pressure P.

Subsequently, Equation (27b) is integrated with respect to r, on the surface of charged bubble, where supposing $v(r,t) = \frac{dR}{dt}$ and $R(r \to \infty, t) = 0$, then:

$$v = \frac{1}{r^2}(R^2 \frac{dR}{dt}). \tag{28}$$

In the following, using Equation (28) into Equation (27a), and supposing $(r \to \infty, t = 0)$, hence, integrating the results, t, we obtain:

$$P = \frac{\rho}{r}\frac{d}{dt}\left(R^2\frac{dR}{dt}\right) + O(\frac{1}{r^4}) \cong \frac{\rho}{r}\frac{d}{dt}\left(R^2\frac{dS}{dt}\right). \tag{29}$$

Noting that, the term $O(\frac{1}{r^4})$ is omitted because of the high order of $(\frac{1}{r^4})$, and the pressure charged fluid in Equation (27a) is the pressure caused by each charged bubble. In this approach, the subscripts i and j are used for the individual effects of each charged bubble (i.e., the interaction between i- and j- charged bubbles). Thus, the interparticle pressure is obtained as follows:

$$P_{\text{int}} = \sum_{J=1,J\neq i}^{2} P_j = \rho_l \sum_{J=1,J\neq i}^{N} \frac{1}{r_j}\frac{d}{dt}\left(R_j^2\left(\frac{dR_j}{dt}\right)\right). \tag{30}$$

It is supposed that the charged bubbles' centres remain unconverted and unaltered. For completing the calculations, interparticle interactions can occur between two charged bubbles, i.e., identical charged bubbles with the same distance and conditions:

$$R_i = R \text{ and } H = \sum_{J=2,}^{N}\left(\frac{1}{r_{1,j}}\right)^{-1}, \text{ for } i,j = 1,2,\ldots,N \text{ and } i \neq j.$$

On the other hand, due to the charged bubbles having the same dynamics, H defines the distance between the centers of the charged bubbles: N is the number of charged bubbles. Consequently, we obtained:

$$P_{\text{int}} \to \frac{\rho}{H}(N-1)\frac{d}{dt}\left(R^2\frac{dR}{dt}\right), N = 1,2,3,\ldots. \tag{31}$$

Again, H and N are the distance between each pair of charged cavitation bubbles and the number of charged cavitation bubble, respectively.

Combining Equations (8) and (31), the charged-Rayleigh–Plesset model in dielectric liquid, considering interparticle interaction of the cavitation bubbles, becomes:

$$R\ddot{R} + \frac{3}{2}\dot{R}^2 = \frac{1}{\rho}\left(\left(P_v - P_0 + \frac{2\sigma}{R_0} - \frac{Q^2}{8\pi\varepsilon R_0^4}\right)\left(\frac{R_0}{R}\right)^{3\kappa} - \frac{2}{R}\sigma - 4\frac{\rho\dot{R}}{R}\eta + \frac{Q^2}{8\pi\varepsilon R^4} + (P_v - P_0) - \frac{\rho}{H}(N-1)\frac{d}{dt}\left(R^2\frac{dR}{dt}\right)\right) \tag{32}$$

Again, applying this relation $\frac{d}{dt}\left(R^2\frac{dR}{dt}\right) = R^2\ddot{R} + 2R\dot{R}^2$ and the pressure $P_g(t)$ into Equation (32), the charged multibubbles under the effect of interparticle interactions between bubbles becomes:

$$\frac{d}{dt}\left(R^2\frac{dR}{dt}\right) = \frac{1}{\rho}(P_g(t) - P_0) - \frac{Q^2}{8\pi\rho\varepsilon R_0^4}\left(\frac{R_0}{R}\right)^{3\kappa} - 4\frac{\dot{R}}{R}\eta - \frac{2}{\rho R}\sigma + \frac{Q^2}{8\pi\rho\varepsilon R^4} + \frac{1}{\rho}P_v - \frac{1}{H}(N-1)\left(R^2\ddot{R} + 2R\dot{R}^2\right) \tag{33}$$

Applying the conditions in Equation (11) into Equation (33), the nonlinear differential equation of charged multibubbles becomes:

$$\frac{1}{2R^2\dot{R}}\frac{d}{dt}\left(R^3\dot{R}^2\right)=\frac{1}{\rho}\left(\frac{\Delta T_B^*}{\Delta T_0}+1\right)\mathbb{ZZ}_2-\frac{Q^2}{8\pi\rho\varepsilon R_0^4}\left(\frac{R_0}{R}\right)^{3\kappa}-4\frac{\dot{R}}{R}\eta-\frac{2}{\rho R}\sigma+\frac{Q^2}{8\pi\rho\varepsilon R^4}+\frac{1}{\rho}P_v-\frac{1}{H}(N-1)\left(R^2\ddot{R}+2R\dot{R}^2\right) \quad (34)$$

Here, $\mathbb{ZZ}_1=\frac{\mathbb{Z}_2}{T_0-T_\infty}$; $\mathbb{ZZ}_2=\frac{3}{2}\rho\dot{R}_0^2+4\frac{\rho\dot{R}_0}{R_0}\eta+\frac{2}{R_0}\sigma-P_v+\frac{2\rho}{H}(N-1)R_0\dot{R}_0^2$, $\Delta T_0=T_0-T_\infty$, and ΔT_T^* were defined in a previous section in (15).

By applying the relation between Equations (17) and (18) into Equation (34), Equation (34) applied to charged multibubbles can be put in a dimensionless equation as:

$$\begin{aligned}\frac{1}{6\Psi'}\frac{d}{d\nu}\left(\Psi^{\frac{7}{3}}\dot{\Psi}^2\right)=\frac{1}{\rho\Omega^2R_0^2}\mathbb{ZZ}_2-\mathbb{ZZ}_3\int_0^\nu\left((\nu-\xi)^{-\frac{1}{2}}\Psi'(\xi)\right)d\xi-\frac{Q^2}{8\pi\rho\varepsilon\Omega^2R_0^2}\left(\frac{1}{\Psi^{\frac{1}{3}}}\right)^{3\kappa}-\frac{4}{3\Omega R_0^2}\Psi^{\frac{1}{3}}\Psi'\eta-\frac{2}{\rho\Omega^2R_0^2}\frac{1}{\Psi^{\frac{1}{3}}}\sigma+\\ \frac{Q^2}{8\pi\rho\varepsilon\Omega^2R_0^2}\frac{1}{\Psi^{\frac{1}{3}}}+\frac{1}{\rho\Omega^2R_0^2}P_v-\frac{1}{H}(N-1)\left(\left(\frac{1}{3}\Psi^{\frac{8}{3}}\Psi''+\frac{2}{9}\Psi^{\frac{5}{3}}\dot{\Psi}^2\right)+\frac{2}{9}R_0\Psi^{\frac{5}{3}}\dot{\Psi}^2\right)\end{aligned} \quad (35)$$

where $\mathbb{ZZ}_3=\left(\frac{\Omega a_l}{9\pi}\right)^{\frac{1}{2}}\frac{\rho_v L\mathbb{ZZ}_2}{\rho\Omega^2\Delta T_0R_0k_l}$.

In the case where charged microbubble dynamics undergo complete growth, the inertial forces are neglected and the boundary conditions in Equation (11) are satisfied, mathematically, then $R(t_m)=R_m, \dot{R}(t_m)=\dot{R}_m, \ddot{R}(t_m)=0$, and $\frac{1}{6\dot{\Psi}}\frac{d}{d\nu}\left(\Psi^{\frac{7}{3}}\dot{\Psi}^2\right)\to 0$. Then, Equation (35) converts to:

$$\begin{aligned}\int_0^\nu\left((\nu-\xi)^{-\frac{1}{2}}\Psi'(\xi)\right)d\xi=\frac{1}{\mathbb{ZZ}_3}\left[\frac{1}{\rho\Omega^2R_0^2}\mathbb{ZZ}_2-\frac{Q^2}{8\pi\rho\varepsilon\Omega^2R_0^2}\left(\frac{1}{\Psi_m^{\frac{1}{3}}}\right)^{3\kappa}-\frac{4}{3\Omega R_0^2}\Psi_m^{\frac{1}{3}}\Psi'_m\eta-\frac{2}{\rho\Omega^2R_0^2}\frac{1}{\Psi_m^{\frac{1}{3}}}\sigma+\frac{Q^2}{8\pi\rho\varepsilon\Omega^2R_0^2}\frac{1}{\Psi_m^{\frac{1}{3}}}+\right.\\ \left.\frac{1}{\rho\Omega^2R_0^2}P_v-\frac{1}{H}(N-1)\left(\left(\Psi_{\mathrm{m}}^{\frac{8}{3}}\Psi''_{\mathrm{m}}+\frac{2}{9}\Psi_{\mathrm{m}}^{\frac{5}{3}}\dot{\Psi}_m^2\right)+\frac{2}{9}R_0\Psi_m^{\frac{5}{3}}\dot{\Psi}_m^2\right)\right]\end{aligned} \quad (36)$$

In order to complete the solution (36), we use these assumptions: $\xi=\xi_1\nu$, and $\beta(\nu)=\gamma\nu^{\frac{1}{2}}$; γ denotes a constant, and the result is:

$$\begin{aligned}\gamma=\frac{2}{\mathbb{ZZ}_3\pi}\left[\frac{1}{\rho\Omega^2R_0^2}\mathbb{ZZ}_2-\frac{Q^2}{8\pi\rho\varepsilon\Omega^2R_0^2}\left(\frac{1}{\Psi_m^{\frac{1}{3}}}\right)^{3\kappa}-\frac{4}{3\Omega R_0^2}\Psi_m^{\frac{1}{3}}\Psi'_m\eta-\frac{2}{\rho\Omega^2R_0^2}\frac{1}{\Psi_m^{\frac{1}{3}}}\sigma+\frac{Q^2}{8\pi\rho\varepsilon\Omega^2R_0^2}\frac{1}{\Psi_m^{\frac{1}{3}}}+\frac{1}{\rho\Omega^2R_0^2}P_v-\right.\\ \left.\frac{1}{H}(N-1)\left(\left(\Psi_{\mathrm{m}}^{\frac{8}{3}}\Psi''_{\mathrm{m}}+\frac{2}{9}\Psi_{\mathrm{m}}^{\frac{5}{3}}\dot{\Psi}_m^2\right)+\frac{2}{9}R_0\Psi_m^{\frac{5}{3}}\dot{\Psi}_m^2\right)\right]\end{aligned} \quad (37)$$

and $\beta(\nu)$ becomes:

$$\begin{aligned}\beta(\nu)=\frac{2}{\mathbb{ZZ}_3\pi}\left[\frac{1}{\rho\Omega^2R_0^2}\mathbb{ZZ}_2-\frac{Q^2}{8\pi\rho\varepsilon\Omega^2R_0^2}\left(\frac{1}{\Psi_m^{\frac{1}{3}}}\right)^{3\kappa}-\frac{4}{3\Omega R_0^2}\Psi_m^{\frac{1}{3}}\Psi'_m\eta-\frac{2}{\rho\Omega^2R_0^2}\frac{1}{\Psi_m^{\frac{1}{3}}}\sigma+\frac{Q^2}{8\pi\rho\varepsilon\Omega^2R_0^2}\frac{1}{\Psi_m^{\frac{1}{3}}}+\frac{1}{\rho\Omega^2R_0^2}P_v-\right.\\ \left.\frac{1}{H}(N-1)\left(\left(\Psi_{\mathrm{m}}^{\frac{8}{3}}\Psi''_{\mathrm{m}}+\frac{2}{9}\Psi_{\mathrm{m}}^{\frac{5}{3}}\dot{\Psi}_m^2\right)+\frac{2}{9}R_0\Psi_m^{\frac{5}{3}}\dot{\Psi}_m^2\right)\right]\nu^{\frac{1}{2}}\end{aligned} \quad (38)$$

Applying Equation (38) into $R=R_0\Psi^{\frac{1}{3}}$, the charged multibubble radius becomes:

$$\begin{aligned}R=R_0\left[\frac{2}{\mathbb{ZZ}_3\pi}\left[\frac{1}{\rho\Omega^2R_0^2}\mathbb{ZZ}_2-\frac{Q^2}{8\pi\rho\varepsilon\Omega^2R_0^2}\left(\frac{1}{\Psi_m^{\frac{1}{3}}}\right)^{3\kappa}-\frac{4}{3\Omega R_0^2}\Psi_m^{\frac{1}{3}}\Psi'_m\eta-\frac{2}{\rho\Omega^2R_0^2}\frac{1}{\Psi_m^{\frac{1}{3}}}\sigma+\frac{Q^2}{8\pi\rho\varepsilon\Omega^2R_0^2}\frac{1}{\Psi_m^{\frac{1}{3}}}+\frac{1}{\rho\Omega^2R_0^2}P_v\right.\right.\\ \left.\left.-\frac{1}{H}(N-1)\left(\left(\Psi_{\mathrm{m}}^{\frac{8}{3}}\Psi''_{\mathrm{m}}+\frac{2}{9}\Psi_{\mathrm{m}}^{\frac{5}{3}}\dot{\Psi}_m^2\right)+\frac{2}{9}R_0\Psi_m^{\frac{5}{3}}\dot{\Psi}_m^2\right)\right]\right]^{1/3}\nu^{\frac{1}{6}}\end{aligned} \quad (39)$$

To introduce ν versus time t, applying Equation (39) into Equation (17), we obtain:

$$\nu^{\frac{1}{6}} = \left(\frac{\Omega}{3}t\right)^{\frac{1}{2}}\left[\frac{2}{\pi\mathbb{Z}\mathbb{Z}_3}\left[\frac{1}{\rho\Omega^2R_0^2}\mathbb{Z}\mathbb{Z}_2 - \frac{Q^2}{8\pi\rho\varepsilon\Omega^2R_0^2}\left(\frac{1}{\Psi_m^{\frac{1}{3}}}\right)^{3\kappa} - \frac{4}{3\Omega R_0^2}\Psi_m^{\frac{1}{3}}\Psi'_m\eta - \frac{2}{\rho\Omega^2R_0^2}\frac{1}{\Psi_m^{\frac{1}{3}}}\sigma + \frac{Q^2}{8\pi\rho\varepsilon\Omega^2R_0^2}\frac{1}{\Psi_m^{\frac{1}{3}}} + \frac{1}{\rho\Omega^2R_0^2}P_v - \frac{1}{H}(N-1)\left(\left(\Psi_m^{\frac{8}{3}}\Psi''_m + \frac{2}{9}\Psi_m^{\frac{5}{3}}\dot{\Psi}_m^2\right) + \frac{2}{9}R_0\Psi_m^{\frac{5}{3}}\dot{\Psi}_m^2\right)\right]\right]^{2/3} \tag{40}$$

After making some simple calculations based on the Jacob number, initial void fraction, and thermal diffusivity, the charged interacting-bubble radius becomes:

$$R = \left[\frac{2}{\mathbb{Z}\mathbb{Z}_3\pi}\left[\frac{1}{\rho\Omega^2R_0^2}\mathbb{Z}\mathbb{Z}_2 - \frac{Q^2}{8\pi\rho\varepsilon\Omega^2R_0^2}(\phi_0)^{\kappa} - \frac{4}{3\Omega R_0^2}\phi_0^{\frac{-1}{3}}\Psi'_m\eta - \frac{2}{\rho\Omega^2R_0^2}\phi_0^{\frac{1}{3}}\sigma + \frac{Q^2}{8\pi\rho\varepsilon\Omega^2R_0^2}\phi_0^{\frac{1}{3}} + \frac{1}{\rho\Omega^2R_0^2}P_v - \frac{1}{H}(N-1)\left(\left(\phi_0^{\frac{-8}{3}}\Psi''_m + \frac{2}{9}\phi_0^{\frac{-5}{3}}\dot{\Psi}_m^2\right) + \frac{2}{9}R_0\phi_0^{\frac{-5}{3}}\dot{\Psi}_m^2\right)\right]\right]^{1/3}\frac{\Omega^2\rho R_0}{\mathbb{Z}_3}\left(\frac{12a_1}{3}\right)^{\frac{1}{2}}J_a t^{\frac{1}{2}} \tag{41}$$

3. Validation and Verification Model

To find evidence for the current mathematical approaches of the charged cavitation bubbles, we begin with Equation (32) for charged cavitation multibubbles in dielectric fluids, considering the impact of the interparticle interaction of charged bubbles, where we use Equation (6) for a single charged cavitation bubble as the distance between the charged bubbles H (or r_{ij}) approaches infinity (means mathematically $H \to \infty$ or $r_{ij} \to \infty$) and is verified by:

$$\lim_{H\to\infty}\frac{(N-1)}{H}\frac{d}{dt}\left(R^2\frac{dR}{dt}\right) \to 0,$$

for $N > 1$, and N is the number of charged bubbles.

Additionally, Equation (6) reduces to the results of the dynamics of a single charged bubble during the growth process in [41], from the method based on Plesset–Zwick transformation [43].

On the other hand, the current results of the noninteracting- and interacting charged cavitation bubbles are introduced in a dielectric liquid with the previous available studies in different fluids, such as experimental data [30], Forster and Zuber model [31], Mohammadein et al. models [32,44], and the Plesset–Zwick model [43], as shown in Table 1. Table 2 shows the models and solutions which were utilized in the present study. Moreover, the obtained results hold greater significance in comprehending the intricate behaviour of charged bubbles in the different industrial and technological domains.

Table 1. Characterization of the current models of charged cavitation bubbles and previous studies [31,32,43,44] during the growth process.

Model	Mathematical Formula	Solution	Description
Current Model (6)	$R\ddot{R} + \frac{3}{2}\dot{R}^2 = \frac{1}{\rho}((P_v - P_0 + \frac{2\sigma}{R_0} - \frac{Q^2}{8\pi\varepsilon R_0^4})(\frac{R_0}{R})^{3\kappa} - \frac{2}{R}\sigma - 4\frac{\rho\dot{R}}{R}\eta + \frac{Q^2}{8\pi\varepsilon R^4} + (P_v - P_0))$	$R = \left[\frac{2}{\mathbb{Z}_3\pi}\left[\frac{1}{\rho\Omega^2R_0^2}\mathbb{Z}_2 - \frac{Q^2}{8\pi\rho\varepsilon\Omega^2R_0^2}(\phi_0)^{\kappa} - \frac{4}{3\Omega R_0^2}\phi_0^{\frac{-1}{3}}\Psi'_m\eta - \frac{2}{\rho\Omega^2R_0^2}\phi_0^{\frac{1}{3}}\sigma + \frac{Q^2}{8\pi\rho\varepsilon\Omega^2R_0^2}\phi_0^{\frac{1}{3}} + \frac{1}{\rho\Omega^2R_0^2}P_v\right]\right]^{1/3}\frac{\Omega^2\rho R_0}{\mathbb{Z}_3}(\frac{12a_1}{3})^{\frac{1}{2}}J_a t^{\frac{1}{2}}$	No n-interaction of charged cavitation bubbles in dielectric liquids
Current Model (31)	$R\ddot{R} + \frac{3}{2}\dot{R}^2 = \frac{1}{\rho}((P_v - P_0 + \frac{2\sigma}{R_0} - \frac{Q^2}{8\pi\varepsilon R_0^4})(\frac{R_0}{R})^{3\kappa} - \frac{2}{R}\sigma - 4\frac{\rho\dot{R}}{R}\eta + \frac{Q^2}{8\pi\varepsilon R^4} + (P_v - P_0) - \frac{\rho}{H}(N-1)\frac{d}{dt}(R^2\frac{dR}{dt}))$	$R(t) = \left[\frac{2}{\mathbb{Z}\mathbb{Z}_3\pi}\left[\frac{1}{\rho\Omega^2R_0^2}\mathbb{Z}\mathbb{Z}_2 - \frac{Q^2}{8\pi\rho\varepsilon\Omega^2R_0^2}(\phi_0)^{\kappa} - \frac{4}{3\Omega R_0^2}\phi_0^{\frac{-1}{3}}\Psi'_m\eta - \frac{2}{\rho\Omega^2R_0^2}\phi_0^{\frac{1}{3}}\sigma + \frac{Q^2}{8\pi\rho\varepsilon\Omega^2R_0^2}\phi_0^{\frac{1}{3}} + \frac{1}{\rho\Omega^2R_0^2}P_v - \frac{1}{H}(N-1)((\phi_0^{\frac{-8}{3}}\Psi_m + \frac{2}{9}\phi_0^{\frac{-5}{3}}\dot{\Psi}_m^2) + \frac{2}{9}R_0\phi_0^{\frac{-5}{3}}\dot{\Psi}_m^2)\right]\right]^{1/3}\frac{\Omega^2\rho R_0}{\mathbb{Z}_3}(\frac{12a_1}{3})^{\frac{1}{2}}J_a t^{\frac{1}{2}}$	Cavitation multibubble in dielectric liquids

Table 1. *Cont.*

Model	Mathematical Formula	Solution	Description
Forster and Zuber model [31]	$R\ddot{R} + \frac{3}{2}\dot{R}^2 = \frac{1}{\rho}((P_v - P_0) - \frac{2}{R}\sigma - 4\frac{\rho\dot{R}}{R}\eta)$	$R(t) = J_a(P\, a_l t)^{\frac{1}{2}}$	Single cavitation bubble in Newtonian fluid
Mohammadein et al. model [44]	$R\ddot{R} + \frac{3}{2}\dot{R}^2 = \Delta P - \frac{2\sigma(t)}{\rho R} - 4\frac{\dot{R}}{R}\eta$	$R(t) = \frac{3\rho R_0 R_0^2 + 8\varepsilon\eta\rho R_0^2 \dot{R}_0 + 4\sigma(1-\phi_0^{\frac{1}{3}})}{3\rho R_0 R_0^2 - 2bR_0\Delta P_0 + 8\varepsilon\eta\dot{R}_0 + 4\sigma} J_a(\frac{12a_l}{\pi}t)^{\frac{1}{2}}$	Single cavitation bubble in Newtonian fluid
Plesset and Zwick model [43]	$R\ddot{R} + \frac{3}{2}\dot{R}^2 = \frac{P(R) - P_0}{\rho}$	$R(t) = J_a(\frac{12a_l}{\pi}t)^{\frac{1}{2}}$	Single cavitation bubble in Newtonian fluid
Mohammadein et al. model [32]	$R\ddot{R} + \frac{3}{2}\dot{R}^2 = \Delta P - \frac{2\sigma(t)}{\rho R}$	$R(t) = \frac{3\rho R_0^2 + 4B_2\rho_g R_0(1-\phi_0^{\frac{1}{3}})}{3\rho R_0^2 - 2b_2\Delta P_0 + 4B_2\rho_g R_0}(\frac{12a_l}{\pi}t)^{\frac{1}{2}}$	Single cavitation bubble in Newtonian fluid

4. Results and Analysis

In this study, the mathematical approaches are formulated and described based on the Rayleigh–Plesset model of charged bubble dynamics in dielectric fluid. The solution of the charged bubble model gives us the analytical solutions and behaviour of noninteracting and interacting charged bubbles. The obtained solutions reveal the main role of physical configuration on the behaviour dynamics of charged cavitation bubbles under the effect of an electric field. To calculate this, the different values of physical configurations (e.g., in refs. [27,42]) are found by: $\rho_l = 1000$ kg.m^{-1}, $\rho_g = 1.308$ kg.m^{-1}, $R_0 = 0.001$ m, $R_{\mathrm{m}} = 0.005$ m, $\dot{R}_0 = 0.1$ m.s^{-1}, $\eta = 0.077$Pas, $\sigma = 0.05$ N.m^{-1}, $C_{PI} = 4179$ J(kg.K)$^{-1}$, $L = 533,000$ J.kg^{-1}, and $k_l = 0.6786$ W.m^{-1}.K^{-1}, $\Delta T_0 = 1.5$ K. The results of the present study on the nonlinear dynamics of charged cavitation bubbles under the effect of an electric field are shown in Figures 2–9, in dielectric liquids where the obtained figures illustrate the influence of the physical parameters as electric charges and polytropic exponents on the growth process of noninteracting and interacting charged cavitation bubbles in dielectric liquids. All graphical representations of the given results are important, not only in explaining the physical configuration of the present model but also in verifying the given solutions. Obtaining this motivation, the given solution in the model's approaches is displayed graphically. All graphical representations of the results are estimated by the symbolic software program (Mathematica software version @13.1), which will be utilized to plot the graphs.

4.1. Effect of Electric Charges and Polytropic Exponent on Charged Cavitation Multibubble Growth

Figure 2 reveals the impact of electric charge Q on growing cavitation bubbles in the dielectric field where the activity of charged cavitation bubbles is increasing with the decrease in electric charge. From that, we obtain the influence of electric charge weakens the growth process of charged cavitation bubbles. On the other hand, Figure 2 shows the comparison between the behaviour of noninteracting and interparticle interaction between charged cavitation bubbles where the growth of noninteracting charged bubbles $(N = 1)$ is higher than in the case of interacting charged bubbles $(N > 1)$. The role of polytropic exponent k on the growth process is shown in Figure 3, where the growth process decreases with the increase in polytropic exponents in dielectric liquids.

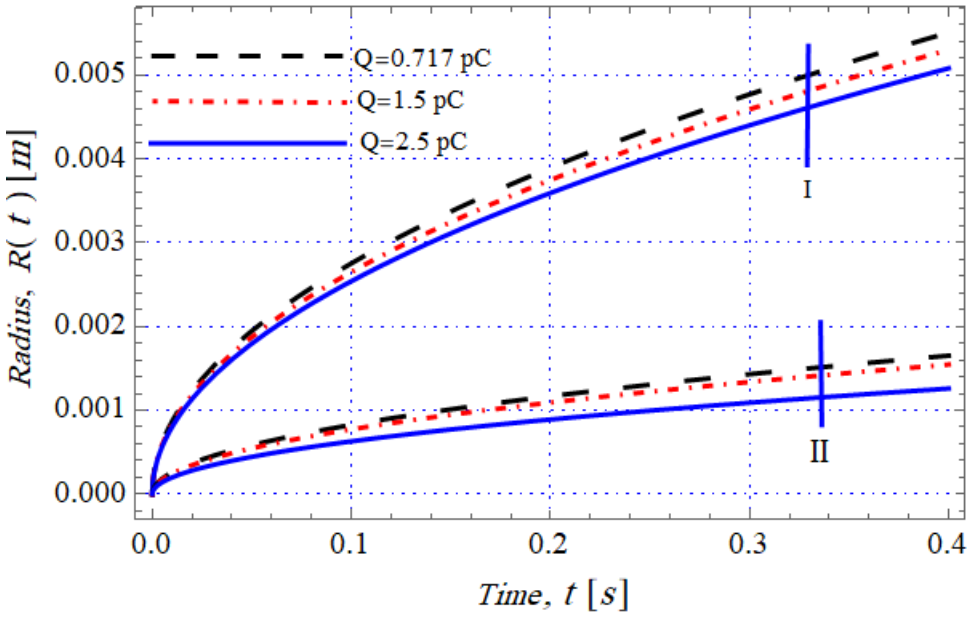

Figure 2. The growth process of charged bubbles dynamics versus time for different values of charged field; I-model of noninteracting bubbles and II-model of interacting bubbles, $H = 0.02$ m, $N = 3$, and $k = 1$.

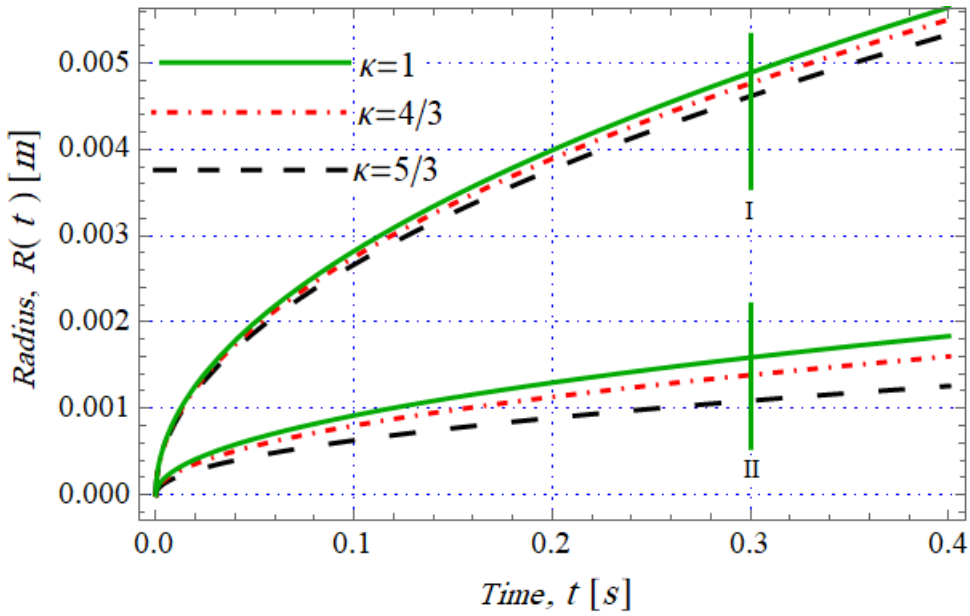

Figure 3. Growth process of charged bubbles dynamics versus time for different values of polytropic exponent; I-model of noninteracting bubbles, and II-model of interacting bubbles, $H = 0.02$ m, $N = 3$.

4.2. Effect of the Number of Charged Bubbles and Charged Bubble–Bubble on Charged Cavitation Multibubble Growth in Dielectric Liquids

Figures 4 and 5 depict the main role of the parameter of the number of cavitation bubbles "N" and the distance between the charged bubbles "H" in our approach, where the increase in the number of bubbles N on the nonlinear cavitation dynamics reduces the behaviour of the growth process. However, the increase in the distance between the charged bubbles on the behaviour of cavitation dynamics significantly enhances the growth process. Figure 6, illustrate the relation between the cavitation radius R and the parameters of the charged field and number of bubbles, respectively, during the growth process at

one instant ($t = 1.0$ s), where it is found that the radii of charged bubbles are inversely proportional to the charged field and the number of bubbles.

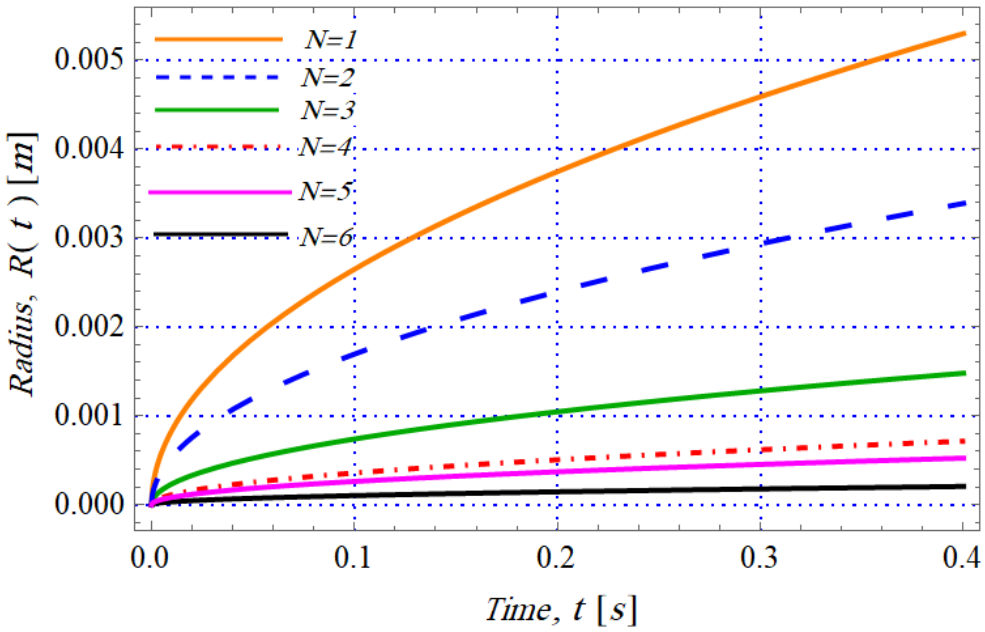

Figure 4. Growth process of charged cavitation multibubble dynamics versus time at the different values of the number of bubbles N. $H = 0.02$ m, $k = 1$.

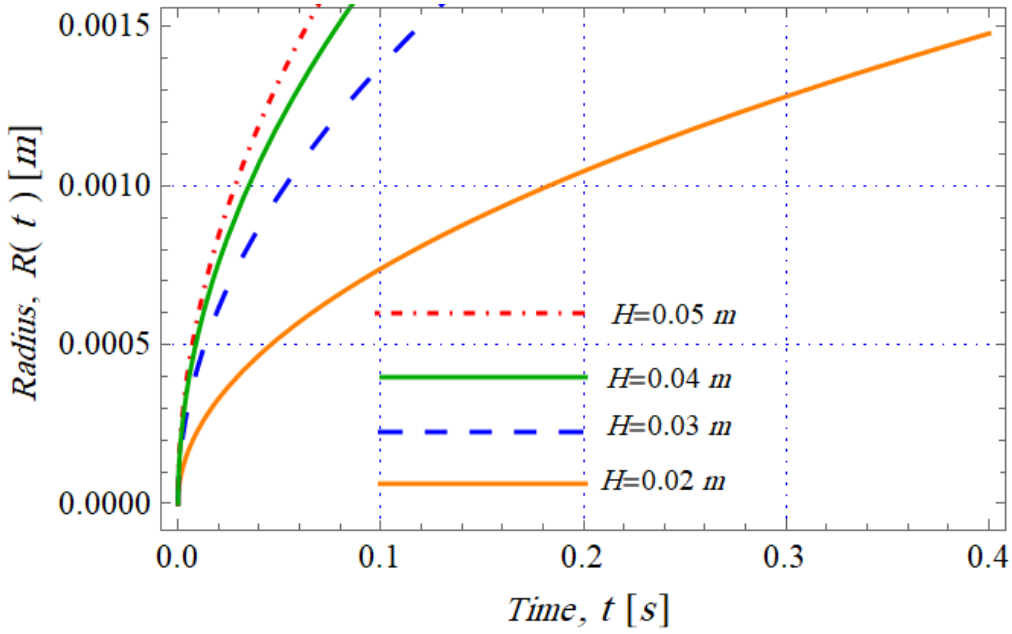

Figure 5. Growth process of charged cavitation multibubble dynamics versus time at the different values of distance between the bubbles, $N = 3$ and $k = 1$.

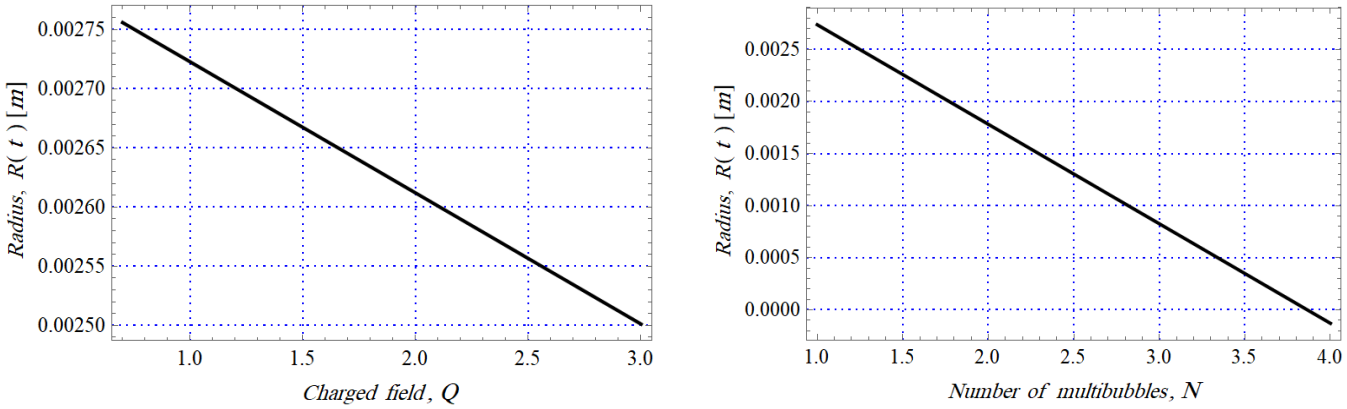

Figure 6. The relation between the cavitation radius R and the parameters charged field and number of multibubbles, respectively, on the growth process at one instant ($t = 1.0$ s).

Figure 7 reveals the results of the single and interparticle interaction of charged cavitation bubbles in a dielectric liquid with the previous available studies in different fluids (as Newtonian liquids (nondielectric liquids), nanofluids) such as experimental data [30], the Forster and Zuber model [31], Mohammadein et al. models [32,44], and the Plesset–Zwick model [43]. These results are the comparison between them. It is found that, firstly, the obtained results agree with the published works in [30–32,43,44]; secondly, the activity of the charged bubbles in the dielectric liquids is significantly lower than in the other published works [30–32,43,44] due to the effects of electric charges.

Ultimately, we recommend using these results when formulating the physicality and modelling of charged bubbles and their applications. It is found that the results obtained give good agreement when compared with experimental and theoretical previous works, and will help the academic community understand the intricate behaviour of charged bubbles in their different industrial and technological applications.

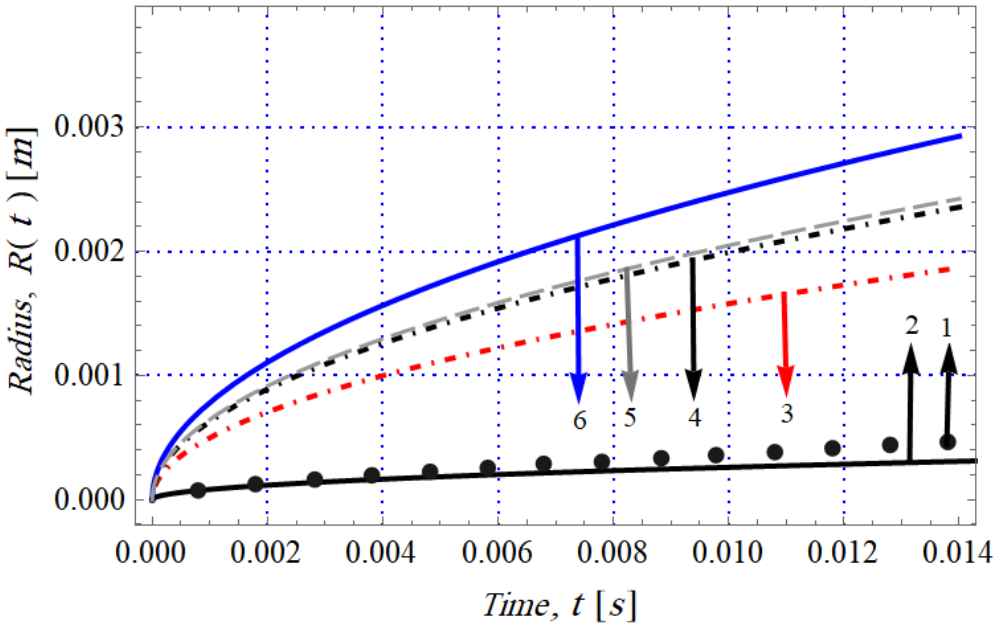

Figure 7. The comparison between the proposed model of the growth process for charged bubble dynamics versus time at $N = 3$, $H = 0.02$ m, black solid line 1: proposed model, line 2: experimental data [30], line 3: Forster and Zuber model [31], line 4: Mohammadein et al. model [44], line 5: Plesset and Zwick model [43], line 6: Mohammadein et al. model [32].

4.3. Effect of the Dimensionless Phase Transition Criteria and Thermal Conductivity on Charged Cavitation Multibubble Growth in Dielectric Liquids

It is notable that dimensionless phase transition criteria (namely, Jacob number $J_a = \frac{\rho C_p \Delta T_0}{\rho_v L}$) is very important in the study the charged bubbles in dielectric liquids. Moreover, the dimensionless phase transition criteria are depended on the value of superheating liquid ΔT_0. So, J_a can be calculated in Table 3 It is noted that the dimensionless phase transition criteria are increasing when the superheating liquid ΔT_0 increase. As following Figure 8, it is noted that the growth process of charged bubbles as a function of time and void fraction is proportional to the dimensionless phase transition criteria J_a. From the results of Table 3 and Figure 8, we obtain the dimensionless phase transition criteria is a dominant of the growth layers of charged bubbles under effect of interparticle interaction of charged bubbles in dielectric liquids. Figure 9 shows the growth process of charged bubbles' dynamics versus time and initial void fraction with different values of thermal diffusivity. We find that the layers of growth of a charged cavitation bubble is proportional to the thermal conductivity k_l. Consequently, an increase in the dimensionless phase transition criterion and thermal conductivity enhances the growth process of charged multiple cavitation bubbles in dielectric liquids.

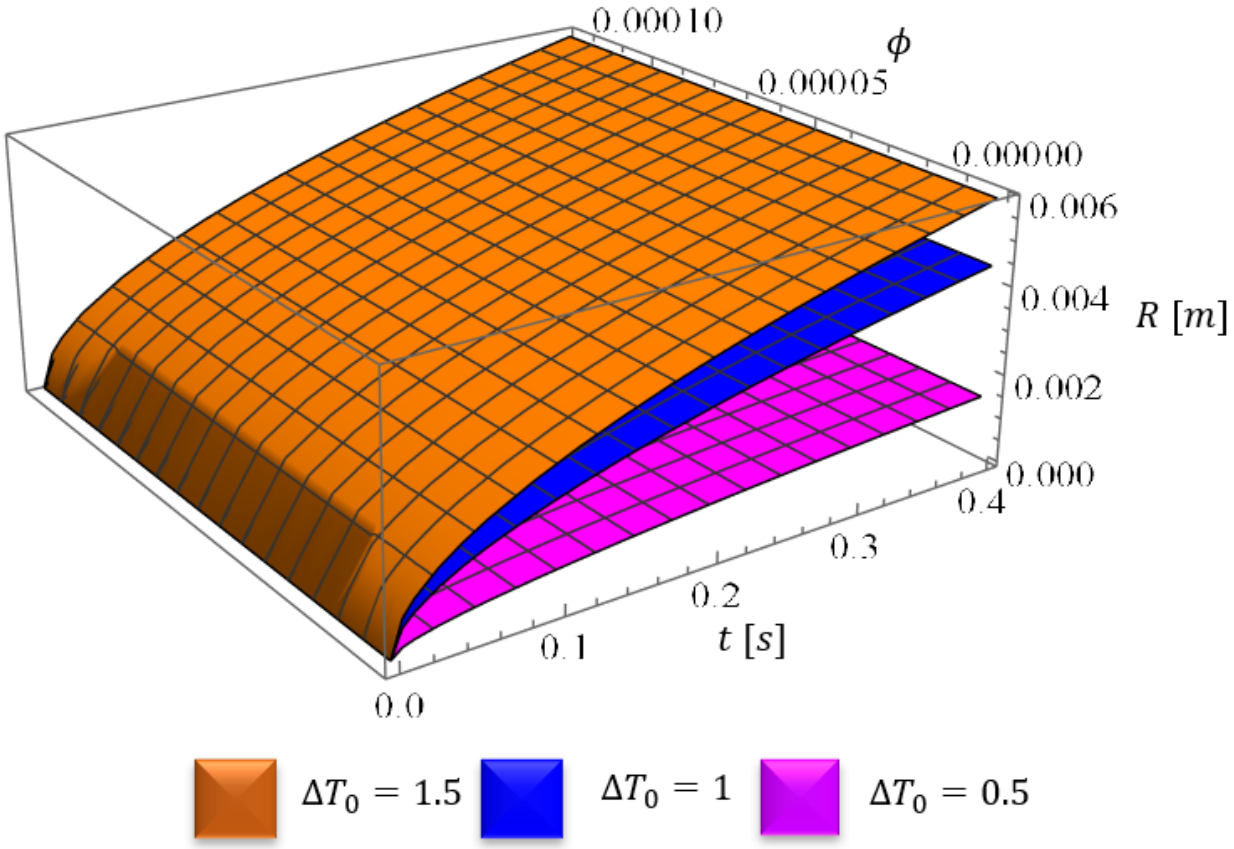

Figure 8. The growth process of charged bubbles' dynamics versus time and initial void fraction at different values of superheating liquid ΔT_0.

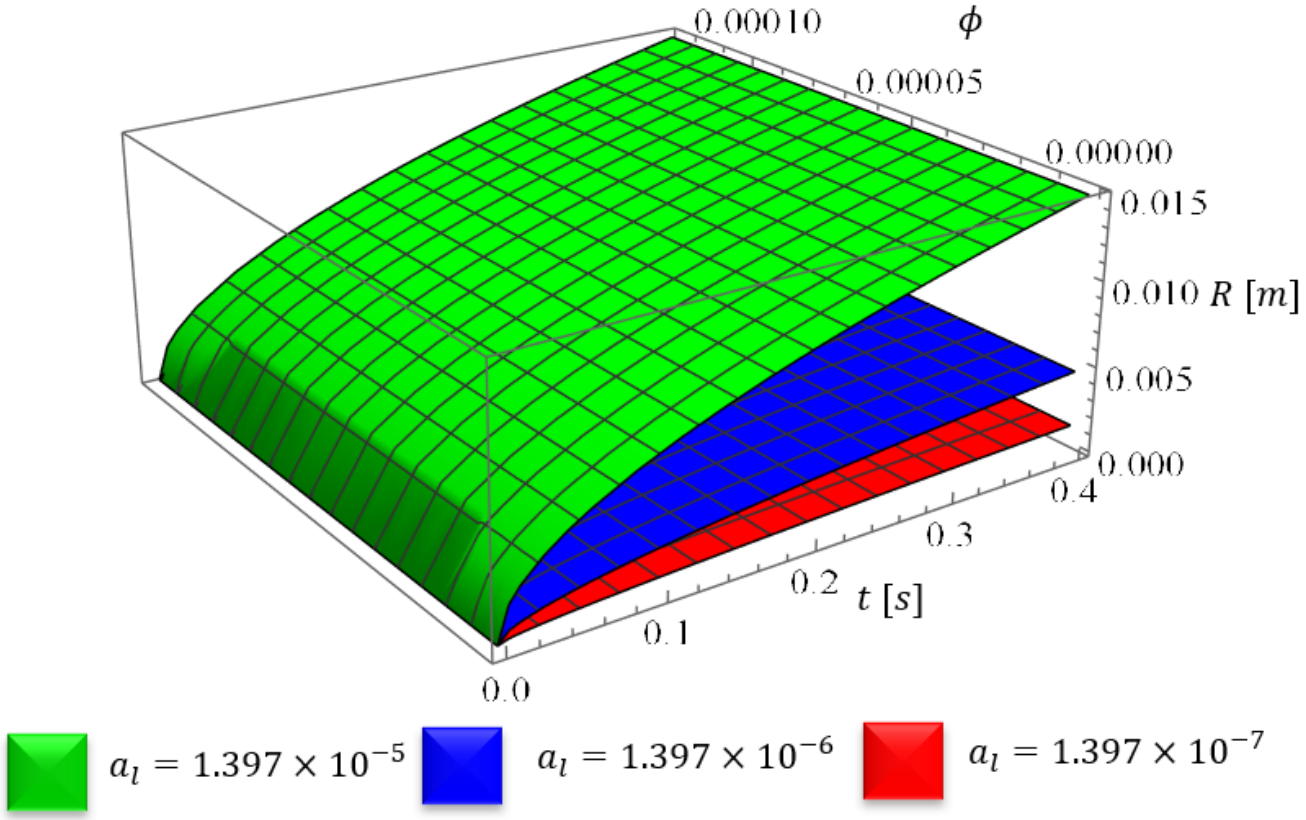

Figure 9. The growth process of charged bubble dynamics versus time and the initial void fraction at different values of thermal diffusivity a_l.

4.4. Estimation the Proposed Different Pressures during the Growth Behaviour of Charged Cavitation Multibubbles in Dielectric Liquids

In this subsection, the proposed different pressures are estimated during the growth behaviour of charged cavitation multibubbles in dielectric liquids. Table 3 illustrates the effect of the growth process on the different pressures such as pressure due to polytropic effects P_k, pressure due to the surface tension P_σ, pressure due to viscous forces P_η, and charged pressure P_Q by permeability, which were stated in Equations (2)–(5), respectively.

Table 2. Numerical calculations of various pressures for nonlinear bubble dynamics in dielectric fields.

	P_k		P_σ		P_Q	
t	**Single Charged Bubble** $N = 1$	**Charged Multibubbles** $N = 2$	**Single Charged Bubble** $N = 1$	**Charged Multibubbles** $N = 2$	**Single Charged Bubble** $N = 1$	**Charged Multibubbles** $N = 2$
0.1	-3.51×10^{15}	-1.61×10^{16}	30.91	110.78	1.08×10^{18}	1.792×10^{20}
0.2	-1.24×10^{15}	-5.72×10^{16}	21.85	78.33	2.71×10^{17}	4.48×10^{19}
0.3	-6.77×10^{14}	-3.11×10^{16}	17.84	63.95	1.21×10^{17}	1.99×10^{19}
0.4	-4.39×10^{14}	-2.02×10^{16}	15.45	55.39	6.79×10^{16}	1.12×10^{19}
0.5	-3.14×10^{14}	-1.44×10^{16}	13.82	49.54	4.35×10^{16}	7.16×10^{18}
0.6	-2.39×10^{14}	-1.11×10^{16}	12.62	45.23	3.02×10^{16}	4.97×10^{18}
0.7	-1.89×10^{14}	-8.73×10^{15}	11.68	41.87	2.21×10^{16}	3.65×10^{18}
0.8	-1.55×10^{14}	-7.15×10^{15}	10.93	39.16	1.69×10^{16}	2.81×10^{18}

Table 3. a: Calculations of dimensionless phase transition criteria, J_a based on superheating liquids ΔT_0. b: calculations of thermal diffusivity, a_l based on thermal conductivity k_l.

a			
ΔT_0 [K]	1.0	1.5	2.0
Dimensionless phase transition criteria, J_a	12.47	18.71	24.95
b			
$k_l[J/(s\ m\ K)$	0.613	0.713	0.813
Thermal diffusivity, $a_l\ [m^2/s]$	1.397×10^{-7}	1.624×10^{-7}	1.852×10^{-7}

5. Conclusions

The nonlinear dynamics models of charged cavitation bubbles and their results for the growth process in dielectric liquids are formulated and solved analytically based on the Plesset–Zwick method. We conclude that:

- The impact of electric charge on growing charged cavitation bubbles reduces the growth process.
- The behaviour of the noninteracting charged cavitation bubbles is higher than in the case of interacting charged cavitation bubbles in dielectric liquids.
- The polytropic exponent weakens the growth process of charged bubbles in dielectric liquids.
- An increase in the dimensionless phase transition criterion and thermal diffusivity enhances the growth process of charged multiple cavitation bubbles in dielectric liquids during the growth process.
- The obtained results of noninteracting and interacting charged cavitation bubbles models in dielectric liquids agree with the published works [30–32,43,44] for different types of the fluids.

The obtained findings would be significant in understanding the complex behaviour of charged cavitation bubbles in practical applications, especially when considering the charged surface tension. Moreover, the current results should be taken into consideration at organization of interacting charged cavitation bubbles and their applications.

Author Contributions: A.K.A.-N.: writing—original draft preparation, methodology, review and editing, software, supervision, validation, conceptualization, formal analysis, and data curation; A.M.H.: writing—original draft preparation, methodology, review and editing, software, validation, conceptualization, formal analysis, and data curation; A.F.A.-B.: writing—original draft preparation, methodology, review and editing, software, supervision, validation, conceptualization, formal analysis, and data curation. All authors have read and agreed to the published version of the manuscript.

Funding: This paper is based upon work supported by Science, Technology & Innovation Funding Authority (STDF) under grant number 48262.

Data Availability Statement: Data are contained within the article.

Conflicts of Interest: The authors declare no conflict of interest.

Nomenclature

Nomenclature

Parameter	Description	Unit
P	Pressure	$N.m^{-2}$
Q	Charge	pC
σ	Surface tension of liquid surrounding the bubble	$N.m^{-1}$
η	Viscosity tension of liquid surrounding the bubble	Pa.s
T	Temperature	K

ε	Permittivity	–
κ	Polytropic coefficient	–
$\Delta T_0 = T_0 - T_\infty$	Initial temperature difference	K
$\Delta T_B^* = T_b$-T_0	The temperature difference defined by Equation (15)	K
a_l	Thermal diffusivity of the liquid	$m^2.s^{-1}$
k	Thermal conductivity	$W.m^{-1}.K^{-1}$
ρ	Density	$Kg.m^{-3}$
ρ_l	Density of the liquid surrounding the bubble	$Kg.m^{-2}$
Ψ	Dimensionless volume variable defined by Equation (17)	–
$\mathbb{Z}_1, \mathbb{Z}_2, \mathbb{Z}_3$	Constants are defined in Equations (12) and (19)	–
$\mathbb{ZZ}_1, \mathbb{ZZ}_2, \mathbb{ZZ}_3$	Constants are defined in Equations (34) and (35)	–
R	Charged bubble radius	m
$\dot{R}$	Instantaneous bubble wall velocity	$m.s^{-1}$
$\ddot{R}$	Instantaneous bubble wall acceleration	$m.s^{-2}$
N	Number of bubbles	–
H	Distance between the bubbles	–
ϕ_0	Initial void fraction defined by Equation (26)	–
J_a	Jacob number given by Equation (26)	–
∇	Del operator	
Subscripts		
b	Boundary	
s	Saturation	
l	Liquid	
g	Gas	
0	Initial	
m	maximum	

References

1. Zhang, A.; Li, S.; Cui, P.; Li, S.; Lium, Y. A unified theory for bubble dynamics. *Phys. Fluids* **2023**, *35*, 033323. [CrossRef]
2. Rayleigh, L. On the pressure developed in a liquid during the collapse of a spherical cavity. *Philos. Mag.* **1917**, *34*, 94–98. [CrossRef]
3. Lauterborn, W.; Kurz, T. Physics of bubble oscillations. *Rep. Progr. Phys.* **2010**, *73*, 106501. [CrossRef]
4. Abu-Nab, A.K.; Omran, M.H.; Abu-Bakr, A.F. Theoretical analysis of pressure relaxation time in N-dimensional thermally-limited bubble dynamics in Fe_3O_4/water nanofluids. *J. Nanofluids* **2022**, *11*, 410–417. [CrossRef]
5. Bai, L.; Xu, W.; Deng, J.; Li, C.; Xu, D.; Gao, Y. Generation and control of acoustic cavitation structure. *Ultrason. Sonochem.* **2014**, *21*, 1696–1706. [CrossRef] [PubMed]
6. Abu-Bakr, A.F.; Abu-Nab, A.K. Towards a laser-induced microbubble during lithotripsy process in soft tissue. *Bull. Russ. Acad. Sci. Phys.* **2022**, *86* (Suppl. S1), S1–S7. [CrossRef]
7. Stride, E.; Coussios, C. Nucleation, mapping and control of cavitation for drug delivery. *Nat. Rev. Phys.* **2019**, *1*, 495–509. [CrossRef]
8. Dollet, B.; Marmottant, P.; Garbin, V. Bubble dynamics in soft and biological matter. *Annu. Rev. Fluid Mech.* **2019**, *51*, 331–355. [CrossRef]
9. Pahk, K.; Gelat, P.; Kim, H.; Saffari, N. Bubble dynamics in boiling histotripsy. *Ultrasound Med. Biol.* **2018**, *44*, 2673–2696. [CrossRef]
10. Abu-Nab, A.K.; Mohamed, K.G.; Abu-Bakr, A.F. Microcavitation dynamics in viscoelastic tissue during histotripsy process. *J. Phys. Condens. Matter.* **2022**, *34*, 304005. [CrossRef]
11. Abu-Nab, A.K.; Mohamed, K.G.; Abu-Bakr, A.F. An analytical approach for microbubble dynamics in histotripsy based on a neo-Hookean model. *Arch. Appl. Mech.* **2023**, *93*, 1565–1577. [CrossRef]
12. Abu-Bakr, A.F.; Mohamed, K.G.; Abu-Nab, A.K. Physico-mathematical models for interacting microbubble clouds during histotripsy. *Eur. Phys. J. Spec. Top.* **2023**, *232*, 1225–1245. [CrossRef]
13. Landel, J.R.; Wilson, D.I. The fluid mechanics of cleaning and decontamination of surfaces. *Annu. Rev. Fluid Mech.* **2021**, *53*, 147–171. [CrossRef]
14. Gaitan, D.; Crum, L.; Church, C.; Roy, R. Sonoluminescence and bubble dynamics for a single, stable, cavitation bubble. *J. Acoust. Soc. Am.* **1992**, *91*, 3166–3183. [CrossRef]
15. Lohse, D. Fundamental fluid dynamics challenges in inkjet printing. *Annu. Rev. Fluid Mech.* **2022**, *54*, 349–382. [CrossRef]
16. Wu, S.; Zuo, Z.; Stone, H.A.; Liu, S. Motion of a free-settling spherical particle driven by a laser-induced bubble. *Phys. Rev. Lett.* **2017**, *119*, 084501. [CrossRef] [PubMed]
17. De Graaf, K.L.; Brandner, P.A.; Penesis, I. Bubble dynamics of a seismic airgun. *Exp. Therm. Fluid Sci.* **2014**, *55*, 228–238. [CrossRef]

18. Goh, B.; Gong, S.; Ohl, S.-W.; Khoo, B.C. Spark-generated bubble near an elastic sphere. *Int. J. Multiph. Flow* **2017**, *90*, 156–166. [CrossRef]
19. Kluesner, J.; Brothers, D.; Hart, P.; Miller, N.; Hatcher, G. Practical approaches to maximizing the resolution of sparker seismic reflection data. *Mar. Geophys. Res.* **2019**, *40*, 279–301. [CrossRef]
20. Plesset, M. The dynamics of cavitation bubbles. *J. Appl. Mech.* **1949**, *16*, 277–282. [CrossRef]
21. Keller, J.; Miksis, K. Bubble oscillations of large amplitude. *J. Acoust. Soc. Am.* **1980**, *68*, 628. [CrossRef]
22. Prosperetti, A.; Lezzi, A. Bubble dynamics in a compressible liquid—Part 1: First-order theory. *J. Fluid Mech.* **1986**, *168*, 457–478. [CrossRef]
23. Lezzi, A.; Prosperetti, A. Bubble dynamics in a compressible liquid—Part 2: Second-order theory. *J. Fluid Mech.* **1987**, *185*, 289–321. [CrossRef]
24. Herring, C. *Theory of the Pulsations of the Gas Bubble Produced by an Underwater Explosion*; Columbia University, Division of National Defense Research: New York, NY, USA, 1941.
25. Trilling, L. The collapse and rebound of a gas bubble. *J. Appl. Phys.* **1952**, *23*, 14–17. [CrossRef]
26. Keller, J.; Kolodner, I.I. Damping of underwater explosion bubble oscillations. *J. Appl. Phys.* **1956**, *27*, 1152. [CrossRef]
27. Abu-Nab, A.K.; Elgammal, M.I.; Abu-Bakr, A.F. Bubble growth in generalized-Newtonian fluid at low-Mach number under influence of magnetic field. *J. Thermophys. Heat Trans.* **2022**, *36*, 485–491. [CrossRef]
28. Sun, S.; Chen, F.; Zhao, M. Numerical simulation and analysis of the underwater implosion of spherical hollow ceramic pressure hulls in 11,000 m depth. *J. Ocean Eng. Sci.* **2022**, *8*, 181–195. [CrossRef]
29. Mohammadein, S.A. The derivation of thermal relaxation time between two-phase bubbly flow. *Heat Mass Transf.* **2006**, *42*, 364–369. [CrossRef]
30. Dergarabedian, P. The rate of growth of vapor bubbles superheated water. *J. Appl. Mech.* **1953**, *20*, 537–545. [CrossRef]
31. Forster, H.K.; Zuber, N. Growth of a vapor bubble in a superheated liquid. *J. Appl. Phys.* **1954**, *25*, 474–478. [CrossRef]
32. Mohammadein, S.A.; Mohammed, K.G. Growth of a gas bubble in a supersaturated liquid under the effect of variant cases of surface tension. *Int. J. Mod. Phys.* **2011**, *25*, 3053–3070. [CrossRef]
33. Olek, S.; Zvirin, Y.; Elias, E. Bubble growth predictions by the hyperbolic and parabolic heat conduction equations. *Warme-Stoffabertragung* **1990**, *25*, 17–26. [CrossRef]
34. Atkinson, A.J.; Apul, O.G.; Schneider, O.; Garcia-Segura, S.; Westerhoff, P. Nanobubble technologies offer opportunities to improve water treatment. *Acc. Chem. Res.* **2019**, *52*, 1196–1205. [CrossRef] [PubMed]
35. McTaggart, H.A. The electrification at liquid-gas surfaces. *Philos. Mag.* **1914**, *27*, 297–314. [CrossRef]
36. Alty, T. The origin of the electrical charge on small particles in water. *Proc. R. Soc. Lond A* **1926**, *112*, 235–251.
37. Dastgheyb, S.S.; Eisenbrey, J.R. Microbubble applications in biomedicine, Handbook of Polymer Applications in Medicine and Medical Devices. In *Plastics Design Library*; William Andrew Publishing: Oxford, UK, 2014; Volume 11, pp. 253–277.
38. Thi Phan, K.K.; Truong, T.; Wang, Y.; Bhandari, B. Nanobubbles: Fundamental characteristics and applications in food processing. *Trends Food Sci. Technol.* **2020**, *95*, 118–130. [CrossRef]
39. Hongray, T.; Ashok, A.; Balakrishnan, J. Effect of charge on the dynamics of an acoustically forced bubble. *Nonlinearity* **2014**, *27*, 1157–1179. [CrossRef]
40. Grigor'ev, A.I.; Zharov, A.N. Stability of the equilibrium states of a charged bubble in a dielectric liquid. *Tech. Phys.* **2000**, *45*, 389–395. [CrossRef]
41. Mohammadein, S.A.; El-Rab, R.A.G. The growth of vapour bubbles in superheated water between two finite boundaries. *Can. J. Phys.* **2001**, *79*, 1021–1029. [CrossRef]
42. Mohammadein, S.A.; Shalaby, G.A.; Abu-Bakr, A.F.; Abu-Nab, A.K. Analytical solution of gas bubble dynamics between two-phase flow. *Res. Phys.* **2017**, *7*, 2396–2403. [CrossRef]
43. Plesset, M.; Zwick, S. The growth of vapor bubbles in superheated liquids. *J. Appl. Phys.* **1954**, *25*, 493–500. [CrossRef]
44. Mohammadein, S.A.; Mohamed, K.G. Growth of a vapour bubble in a viscous, superheated liquid in two phase flow. *Can. J. Phys.* **2015**, *93*, 769–775. [CrossRef]
45. Khojasteh-Manesh, M.M. Numerical investigation of the effect of bubble-bubble interaction on the power of propagated pressure waves. *J. Appl. Comput. Mech.* **2019**, *5*, 181–191.